Nonlinear Effects of Radio over Fiber Transmission in Base Station Cooperation Systems

F. Casal Ribeiro[(1,2)], J. Guerreiro[(1)], R. Dinis[(1,3)], F. Cercas[(1,2)], A. Silva[(1,4)], Armando N. Pinto[(1,4)]
[(1)] IT - Instituto de Telecomunicações, Portugal
[(2)] ISCTE - Instituto Universitário de Lisboa, Portugal
[(3)] FCT - Universidade Nova de Lisboa, Portugal
[(4)] DETI - Universidade de Aveiro, Portugal

***Abstract*—In this paper we consider the uplink of Base Station (BS cooperation) systems, where each Mobile Terminal (MT) employs a Single-Carrier with Frequency-Domain Equalization (SC-FDE) modulation scheme. The combined signals at each BS are detected and/or separated by a Central Processing Unit (CPU) with Iterative Block Decision Feedback Equalization (IB-DFE) receivers. We consider a Radio-over-Fiber (RoF) link between the BS and the CPU, the electrical and optical conversions are performed by a Mach-Zehnder (MZ) modulator, which introduces nonlinear distortion. We design robust receivers that take advantage of the statistical characteristics of the nonlinear distortion.**[1]

***Index Terms*—Radio over Fiber, nonlinear effects, BS cooperation, SC-FDE, IB-DFE**

I. Introduction

Next generation mobile networks, the fifth generation (5G), will reinforce the need for developing high speed broadband wireless access services [1]. With it, the requirement for better spectral efficiency and interference management is mandatory. Therefore, 5G intends for providing a denser network of mobile terminals in broadband scenarios, as well as a high number of pico and femto cells in a small cells clustered environment. Suited for clustered scenarios and providing significantly improvements in spectral efficiency, base station (BS) cooperation schemes are a logical design for future wireless systems. Contrarily to conventional schemes, where mobile terminals (MTs) employ different frequencies for adjacent cells to avoid intercell interference [2], in BS cooperation MTs can transmit using the same physical channel, allowing universal frequency reuse. Subsequently, the received combined signals at a given BS are sent to a central processing unit (CPU) that performs the separation of the signals associated to different MTs. Block transmission techniques, combined with frequency-domain processing, are proved to be highly robust for broadband cellular systems such as BS cooperation. These approaches include orthogonal frequency division multiplexing (OFDM) [3] and single-carrier with frequency domain equalization (SC-FDE) [4]. SC-FDE and OFDM modulations present identical overall signal processing requirements and performance, yet, the envelope fluctuations of OFDM signals are much higher when compared to the ones of SC-FDE, indicating that OFDM and SC-FDE are preferable for the downlink and uplink transmissions, respectively [5], [6].

One promising approach to provide broadband wireless services is a radio-over-fiber (RoF) transmission system, which uses radio frequency signals through the optical fiber [7]. In RoF systems, it is possible to use the millimeter-wave bands in short wireless links on the end of local fiber optic cables, having the transmission of radio signals over fiber between the BSs and central units. Furthermore, the received combined signals from the different MTs are detected and/or separated by implementing iterative receivers based on the IB-DFE concept [8].

This paper considers the uplink of BS cooperation systems where each MT employs a SC-FDE modulation scheme [9]. The combined signals received at a given BS are sent to a CPU via RoF technology, in which the electro-optic and optic-electric conversions are done through a Mach-Zehnder (MZ) modulator [10]. Moreover, the RoF link from the BS and CPU can be modulated as a bandpass memoryless nonlinearity. We design efficient robust receivers that can account for the spectral characterization of the nonlinear distortion introduced by the process of electrical and optical conversions.

This paper is organized as follows: Section II describes the adopted system and Section IV is concerned with the receiver design. Section V presents and evaluates a set of performance results and Section VI concludes the paper.

In this paper we adopt the following notations: bold upper case letters denote matrices or vectors; $\mathbf{I}_N$ denotes the $N \times N$ identity matrix; $\mathbf{x}^*$, $\mathbf{x}^T$ and $\mathbf{x}^H$ denote complex conjugate, transpose and hermitian (complex conjugate transpose) of $\mathbf{x}$, respectively. In general, lower case letters denote time-domain variables and upper case letters denote frequency-domain variables; $\tilde{x}$, $\hat{x}$ and $\bar{x}$ denote sample, "hard decision" and "soft decision" estimates of x, respectively. The expectation of x is denoted by $\mathbb{E}[x]$.

[1]This work is funded by FCT/MEC and Instituto de Telecomunicações through project UID/EEA/50008/2013 (projects PURE-5GNET and OPTICAL-5G).

II. System characterization

A. Radio Link

Fig. 1 illustrates the cellular system adopted in this paper. It is characterized by P MTs transmitting independent data

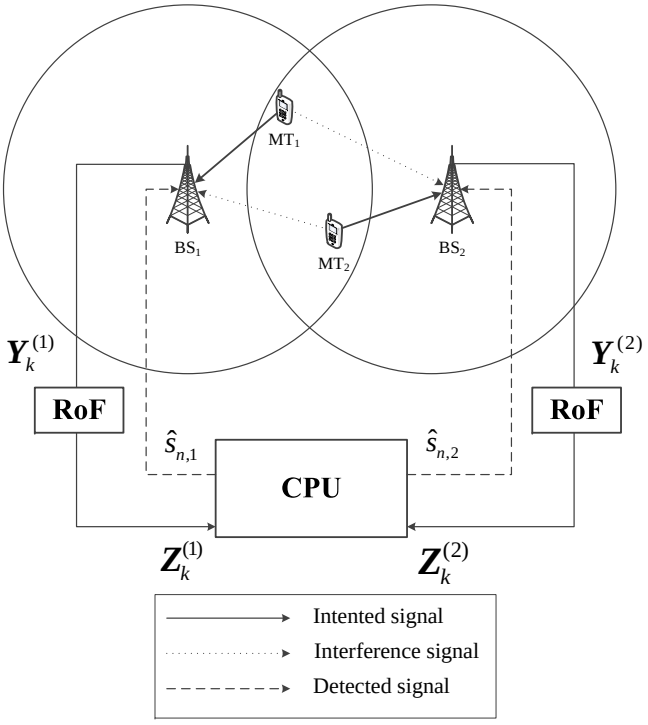

Fig. 1. Adopted cellular scenario.

streams up to R BSs and sharing the same physical channel, that present strong frequency-selectivity . As a BS cooperation scheme, at each BS the combined signals are considered as useful instead of having one MT assigned exclusively to a given BS and the signals from other MTs being considered interference. The subsequent separation of different signals is performed in a central unit after being sent by each BS by a RoF link. Each MT employs an SC-FDE modulation with block size N and quadrature phase shift keying (QPSK) modulations with Gray mapping. The data transmitted by the pth user is represented as $\mathbf{s}^{(p)} = [s_0^{(p)}\ s_1^{(p)}\ ...\ s_{N-1}^{(p)}]^T$ scheme with an appropriate length cyclic prefix (CP) appended to each block. Through a discrete Fourier transform (DFT), the data block can also be represented as $\mathbf{S}^{(p)} = \text{DFT}\left(\mathbf{s}^{(p)}\right) = [S_0^{(p)}\ S_1^{(p)}\ ...\ S_{N-1}^{(p)}]^T$.

At the rth BS, and after removing the CP samples, the time-domain received data stream are given by $\mathbf{y}^{(r)} = [y_0^{(r)}\ y_1^{(r)}\ ...\ y_{N-1}^{(r)}]^T$, with

$$y_n^{(r)} = \sum_{p=1}^{P} \xi_{p,r} s_n^{(p)} \circledast h_{n,p}^{(r)} + \nu_n^{(r)}, \tag{1}$$

where $\circledast$ indicates cyclic convolution. $s_n^{(p)}$ corresponds to the n transmitted data symbol from the pth user. The channel impulsive response is denoted by $h_{n,p}^{(r)}$ and $\nu_n^{(r)}$ indicates the nth sample associated to additive white Gaussian noise (AWGN) block $\boldsymbol{\nu}^{(r)} = [\nu_0^{(r)}\ \nu_1^{(r)}\ ...\ \nu_{N-1}^{(r)}]^T$, whose the frequency-domain version is $N^{(r)} = \text{DFT}(\boldsymbol{\nu}^{(r)}) = [N_0^{(r)}\ N_1^{(r)}\ ...\ N_{N-1}^{(r)}]^T$. Furthermore, $\xi_{p,r}$ is a weighting parameter that accounts for the combined effects of power control and propagation loss, with the average received power associated with the pth MT at the rth BS corresponding to $|\xi_{p,r}|^2$. In the frequency-domain, (1) can be written as

$$Y_k^{(r)} = \sum_{p=1}^{P} S_{k,p} H_{k,p}^{eq(r)} + N_k^{(r)}, \tag{2}$$

with $Y_k^{(r)}$ denoting the kth component of the DFT of the block $\mathbf{y}^{(r)} = [y_0^{(r)}\ y_1^{(r)}\ ...\ y_{N-1}^{(r)}]^T$ that is $\mathbf{Y}^{(r)} = \text{DFT}\left(\mathbf{y}^{(r)}\right) = [Y_0^{(r)}\ Y_1^{(r)}\ ...\ Y_{N-1}^{(r)}]^T$. $S_{k,p}$ is data transmitted by the pth MT on the kth subcarrier. $N_k^{(r)}$ indicates the frequency-domain noise component associated to the rth antenna and the kth frequency. Moreover,

$$H_{k,p}^{eq(r)} = \xi_{p,r} H_{k,p}^{(r)}, \tag{3}$$

where $H_{k,p}^{(r)}$ denotes the channel frequency response between the pth MT and the rth BS, for the kth frequency (considering a normalized channel frequency response with $\mathbb{E}\left[\left|H_{k,p}^{(r)}\right|^2\right] = 1$). Typically, the channel conditions regarding SC-FDE transmission schemes are severely time-dispersive with rich multipath propagation characteristics. Therefore, the time-domain samples $y_n^{(r)}$ can be viewed as a zero-mean complex Gaussian process expressed by

$$\begin{aligned} 2\sigma_y^{(r)^2} = \mathbb{E}\left[\left|y_n^{(r)}\right|^2\right] &= \sum_{p=1}^{P} |\xi_{p,r}|^2\, \mathbb{E}\left[\left|s_n^{(p)}\right|^2\right] + \mathbb{E}\left[\left|\nu_n^{(r)}\right|^2\right] \\ &= \sum_{p=1}^{P} |\xi_{p,r}|^2\, 2\sigma_s^2 + 2\sigma_\nu^2, \end{aligned} \tag{4}$$

in which

$$\sigma_s^2 = \mathbb{E}\left[\left|\text{Re}\{s_n^{(p)}\}\right|^2\right] = \mathbb{E}\left[\left|\text{Im}\{s_n^{(p)}\}\right|^2\right] \tag{5}$$

and

$$\sigma_\nu^2 = \mathbb{E}\left[\left|\text{Re}\{\nu_n^{(r)}\}\right|^2\right] = \mathbb{E}\left[\left|\text{Im}\{\nu_n^{(r)}\}\right|^2\right], \tag{6}$$

indicates to the symbol's and noise variance, respectively. It should be noted that these two variances are equal for all MTs and BSs.

B. ROF Link

The signal received at the rth BS is then converted to the analog domain[2] giving rise to the signal $y(t)^{(r)}$. In the following, we will ommit the dependence with t for the sake of notation simplicity and sent to the RoF link as can be seen in

[2]In our simulations, we considered an oversampling operation that is enough to represent the nonlinearly distorted signals at the MZ output without aliasing.

Fig. 1. This link is modeled by a bandpass memoryless nonlinearity for the MZ modulator and by a noise originated from the RoF link. The bandpass nonlinearities are characterized by the so-called amplitude modulation-amplitude modulation (AM-AM) and amplitude modulation-phase modulation (AM-PM) conversion functions. Due to higher noise values in the optical-electrical conversions it is necessary to operate in the nonlinear zones. Therefore, when their input is $y^{(r)}$, their output can be shown to be given as [11]

$$\begin{aligned} z^{(r)} &= f\left(y^{(r)}\right) \\ &= A\left(\left|y^{(r)}\right|\right)\exp\left(j\left(\Theta\left(\left|y^{(r)}\right|\right)+\arg\left(y^{(r)}\right)\right)\right), \end{aligned} \quad (7)$$

where the nonlinear functions $A(\cdot)$ and $\Theta(\cdot)$ represent the AM-AM and the AM-PM conversion functions, respectively. In our specific case, the MZ modulator only has AM-AM conversion function, which is given by

$$A\left(\left|y^{(r)}\right|\right) = \begin{cases} A_M \sin\left(\frac{\pi}{2A_M}\left|y^{(r)}\right|\right), & \left|y^{(r)}\right| < A_M \\ A_M, & \left|y^{(r)}\right| \geq A_M, \end{cases} \quad (8)$$

where A_M represents the saturation amplitude. In the following, we will refer to the normalized saturation amplitude A_M/σ_y since the magnitude of the nonlinear distortion effects is governed by this ratio[3]. The variance of the real and imaginary parts of the RoF link is dependent on the output power at saturation, i.e.,

$$\sigma^2_{RoF} = \frac{A_M^2}{K_{RoF}}. \quad (9)$$

Therefore, K_{RoF} is a variable that controls the magnitude of this noise.

III. Analytical Evaluation of Nonlinear Distortion Effects

In this section we characterize the nonlinearly distorted signals associated with the MZ modulator. Taking advantage of the Gaussian approximation for the signals at the MZs' output, we can use the Bussgang's theorem [12]. Under these conditions, the time-domain nonlinearly distorted signal associated to the rth BS can be decomposed by the sum of two uncorrelated components

$$z^{(r)} = \alpha y^{(r)} + d^{(r)}, \quad (10)$$

where $d^{(r)}$ denotes the nonlinear distortion and α denotes a scale factor that can be obtained as

$$\alpha = \frac{\mathbb{E}\left[z^{(r)}y^{*(r)}\right]}{\mathbb{E}\left[\left|y^{(r)2}\right|\right]} = \frac{\mathbb{E}\left[z^{(r)}y^{*(r)}\right]}{2\sigma_y^2}. \quad (11)$$

By defining the autocorrelation of the signal at the input of the MZ modulator as $R_y(\tau)$, it can be shown that autocorrelation of the output signal $R_z(\tau)$ can be computed as [13]

$$R_z(\tau) = \sum_{\gamma=0}^{+\infty} 2P_{2\gamma+1}\frac{(\mathrm{Re}(R_y(\tau)))^{2\gamma+1} + j(\mathrm{Im}(R_y(\tau)))^{2\gamma+1}}{R_y(0)^{2\gamma+1}}, \quad (12)$$

where $P_{2\gamma+1}$ is the power associated to the IMP of order $2\gamma+1$, defined as

$$P_{2\gamma+1} = \frac{\left(\int_{-\infty}^{+\infty} f(y)p(y)H_{2\gamma+1}\left(\frac{y}{\sqrt{2}\sigma_y}\right)dy\right)^2}{2^{2\gamma+1}(2\gamma+1)!}, \quad (13)$$

where $H_{2\gamma+1}(\cdot)$ is the Hermite polynomial of order $2\gamma+1$. The average power spectral density (PSD) is obtained by taking the Fourier transform of the output autocorrelation, i.e., $G_z(f) = \mathrm{DFT}(R_z(\tau))$. Fig. 2 shows the simulated and theoretical PSD associated to a given BS and channel realization considering a MZ modulator with $A_M/\sigma_y = 3.0$. It should be noted that at the MZ output, one

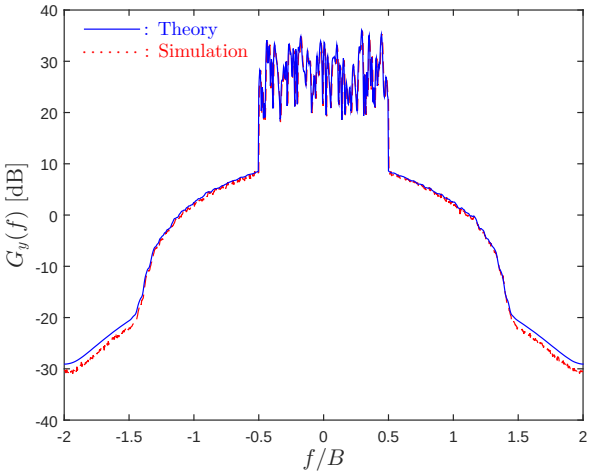

Fig. 2. PSD of nonlinearly distorted signal $z^{(r)}$ considering $A_M/\sigma_y = 3.0$ and a given channel realization.

can also take advantage of the Bussgang's theorem to divide the nonlinearly distorted signal PSD as the sum of two PSDs: one that is proportional to the input signals' PSD and another one that is related to the nonlinear distortion. Therefore, we have

$$G_z(f) = |\alpha|^2 G_y(f) + G_d(f). \quad (14)$$

Fig. 3 shows the simulated and theoretical PSD of the nonlinear distortion term $d^{(r)}$ associated to a given BS and channel realization, considering a MZ modulator with $A_M/\sigma_y = 3.0$. As can be seen in Figs. 2 and 3, our analytical approach allows to obtain very accurate estimates of the PSD associated to the output signals as well as the PSD of the nonlinear distortion term. At the CPU, the received signal is filtered and sampled. Therefore, in the frequency-domain, it can be expressed by $\mathbf{Z}^{(r)} = [Z_0^{(r)}\ Z_1^{(r)}\ \ldots\ Z_{N-1}^{(r)}]^T$

$$Z_k^{(r)} = \alpha Y_k^{(r)} + D_k^{(r)} + W_k^{(r)} \quad (15)$$

[3]Note that as $\sigma_y^{(r)^2}$ is approximately equal for all BS, we ommit the dependence with r and we consider that the variance of the real and imaginary parts of the received signal at a given BS is $2\sigma_y^2$.

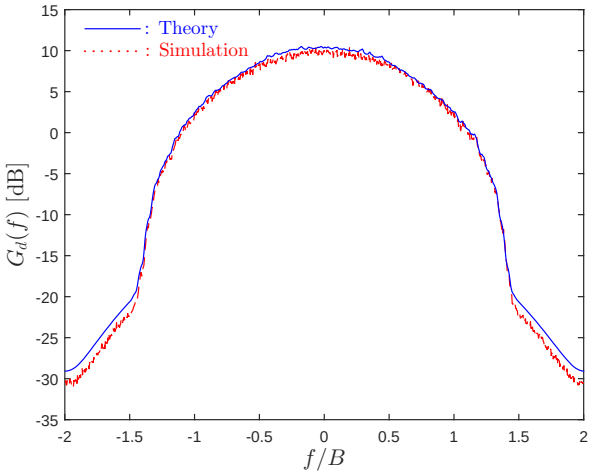

Fig. 3. PSD of the distortion component $d^{(r)}$ considering $A_M/\sigma_y = 3.0$ and a given channel realization.

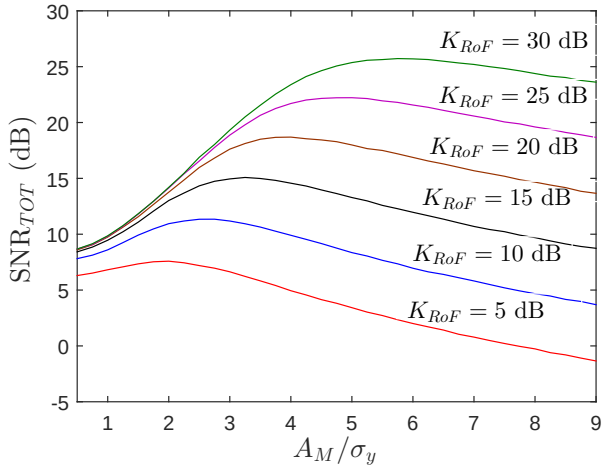

Fig. 4. Evolution of the average SNR_{TOT} considering different values of K_{RoF}.

where $D_k^{(r)}$ and $W_k^{(r)}$ represent the frequency-domain samples associated to the nonlinear distortion and to the noise from the RoF link, that are represented by blocks $\mathbf{D}^{(r)} = [D_0^{(r)}\ D_1^{(r)}\ ...\ D_{N-1}^{(r)}]^T$ and $\mathbf{W}^{(r)} = [W_0^{(r)}\ W_1^{(r)}\ ...\ W_{N-1}^{(r)}]^T$, respectively. Note that the performance will be affected by this two impairments. Thus, by considering the presence of both the nonlinear distortion as well as the noise from the RoF link, one can define the SNR_{TOT} for the kth subcarrier and a given channel realization as

$$\mathrm{SNR}_{TOT\,k} = \frac{|\alpha|^2 \mathbb{E}\left[|Y_k|^2\right]}{\mathbb{E}\left[|D_k|^2\right] + \mathbb{E}\left[|W_k|^2\right]} \tag{16}$$

where it should be noted that $\mathbb{E}\left[|D_k|^2\right] = G_d(k/T) = 2\sigma_D^2(k)$. Fig 4 shows the evolution of the average SNR_{TOT}, average along all the block subcarriers, considering different values of K_{RoF} and different saturation levels. From this figure, it can be observed that, for a given value of K_{RoF}, there is an optimum value of A_M/σ that leads to the lowest SNR_{TOT}. This can be explained by the fact that low values of A_M/σ lead to low values of noise from the RoF link (see 9). However, low values of A_M/σ also mean that the magnitude of the nonlinear distortion is high since it is very likely that the MZ is operating in the nonlinear region. When A_M/σ increases, the operation of the MZ modulator gets more linear and the nonlinear distortion decreases. However, under these conditions, the magnitude of the noise from the RoF link increases which means that SNR_{TOT} decreases. For this reason, there is an optimum level of A_M/σ that will lead to the best performance.

IV. Receiver Design

Fig. 5 illustrates the block diagram regarding the detection process, in which its design is based on the IB-DFE concept [8]. This method allows an efficient detection and/or separation

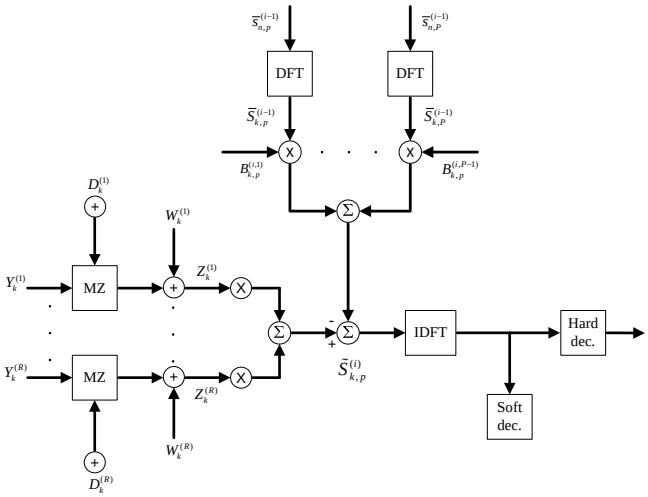

Fig. 5. Multiuser IB-DFE receiver design.

of signals related with the different MTs, taking full advantage of inherent macro-diversity effects while using a single frequency scheme. In each iteration, the MTs are separated in a successive interference cancelation (SIC) method, where the most updated estimate of the transmitted data associated to each user is used to cancel residual interference.

At the ith iteration the estimated data symbols related with the pth user $\{\hat{s}_n^{(p)}\}$ correspond to the hard decisions of the time-domain detector output $\{\tilde{s}_n^{(p)}\} = \mathrm{IDFT}\{\tilde{S}_k^{(p)}\}$, where IDFT indicates the Inverse Discrete Fourier Transform and $\tilde{S}_k^{(p)}$ is expressed as

$$\tilde{S}_{k,p} = \mathbf{F}_{k,p}^T \mathbf{Z}_k - \mathbf{B}_{k,p}^T \bar{\mathbf{S}}_{k,p}. \tag{17}$$

$\mathbf{F}_{k,p}^T = \left[F_{k,p}^{(1)}, ..., F_{k,p}^{(R)}\right]$ and $\mathbf{B}_{k,p}^T = \left[B_{k,p}^{(1)}, ..., B_{k,p}^{(P)}\right]$ denote the feedforward and feedback coefficients, respectively, and define the detector's state at a given iteration. Moreover, $\bar{\mathbf{S}}_{k,p}$ is given by $\bar{\mathbf{S}}_{k,p} = \left[\bar{S}_{k,1}, ..., \bar{S}_{k,p-1}, \bar{S}_{k,p}, ..., \bar{S}_{k,P}\right]^T$, where

$\bar{S}_{k,p}$ corresponds to the DFT of the block of time-domain average values conditioned by the detector output $\bar{s}_{n,p}$.

An improved detection is provided by the computation of the optimal coefficients $\mathbf{F}_{k,p}$ and $\mathbf{B}_{k,p}$. To do so, the minimum mean squared error (MMSE) criterium is employed. For the pth MT and subcarrier k, the MSE for the frequency-domain samples $\tilde{S}_{k,p}$ is given by

$$\Theta_{k,p} = \mathbb{E}\left[\left|\tilde{S}_k^{(p)} - S_k^{(p)}\right|^2\right] = \mathbb{E}\left[\left|\mathbf{F}_{k,p}^T \mathbf{Z}_k - \mathbf{B}_{k,p}^T \bar{\mathbf{S}}_k^{(p)} - S_k^{(p)}\right|^2\right], \tag{18}$$

where its minimization is conditioned to

$$\gamma_p = \frac{1}{N}\sum_{k=0}^{N-1}\sum_{r=1}^{R} F_{k,p}^{(r)} H_{k,p}^{eq(r)} = 1, \tag{19}$$

with γ_p indicating the average overall channel frequency response. Applying the gradient for the Lagrange function as

$$J = \Theta_{k,p} + \lambda\left(\gamma_p - 1\right), \tag{20}$$

the optimum coefficients $\mathbf{F}_k$ and $\mathbf{B}_k$ are given by

$$\mathbf{F}_k = \kappa\left(\mathbf{H}_k^H\left(\mathbf{I}_P - \mathbf{P}^2\right)\mathbf{H}_k + \mathbf{D}_k\right)^{-1}\mathbf{H}_k^H \tag{21}$$

and

$$\mathbf{B}_k = \alpha\mathbf{H}_k\mathbf{F}_k - \mathbf{I}_P, \tag{22}$$

with $\mathbf{D}_k$ corresponding to

$$\mathbf{D}_k = \mathrm{diag}\left(\left\{\frac{|\alpha|^2\,\sigma_N^{(r)^2} + \sigma_D^{(r)^2}(k) + \sigma_{RoF}^{(r)^2}}{|\alpha|^2\,\sigma_S^2}; r = 1, ..., R\right\}\right) \tag{23}$$

and κ selected to ensure that $\gamma_p = 1$, in order to have a normalized FDE with $\mathbb{E}\left[\tilde{s}_n^{(p)}\right] = s_n^{(p)}$. In addition, $\sigma_N^{(r)^2}$ and σ_S^2 represent the variance of the real and imaginary parts of the channel noise and data samples components, respectively.

V. Performance Results

In this section, we present bit error rate (BER) performance results considering the system described in the previous sections. As mentioned, the channels present frequency-selective and multipath propagation characteristics with 64 multipath taps. Furthermore, we consider uncorrelated Rayleigh fading on the different multipath components. In this paper, we assume perfect channel estimation and synchronization. For all P transmitted signals associated to each r antenna we consider $\xi_{p,r} = 0$ dB, $N = 256$ and an appropriate cyclic prefix. In each BER performance result a comparison with the matched filter bound (MFB) is provided.

Firstly, let us consider a BS cooperation transmission scheme with $P = 2$ MTs and $R = 2$ BSs in Fig. 6. The variable that controls the magnitude of the noise from the RoF link correspond to $K_{RoF} = 20$ dB, with saturation level of $A_M = 4$, which is the optimal value for this particular K_{RoF}, as shown in Fig. 4. In this figure one can understand the iterative mechanism and how it can improve the BER evaluation. For simplicity, we only show iterations 1, 2 and 4, since the 3rd iteration does not add relevant information.

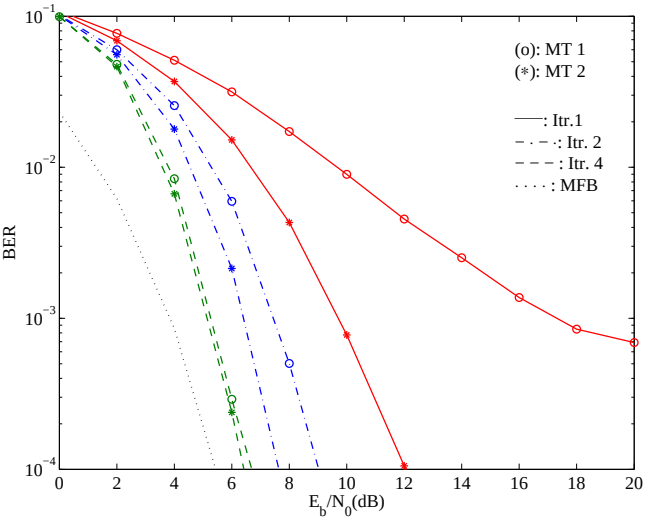

Fig. 6. BER performance for a BS cooperation scenario with $P = 2$ MTs, $R = 2$ BSs, $K_{RoF} = 20$ and optimal $A_M = 4$.

From the results one can notice that the iterative process improves the BER, with a significant change from the first iteration (i.e., linear FDE) to subsequent iterations. Moreover, it can be shown that our receiver can efficiently detect and separate signals from the different MTs, taking advantage of the signal contributions associated with a given MT at each BS. Consequently, the BER performance is very close to the MFB just after 4 iterations.

In order to evaluate the impact of the noise from the RoF link component, let us analyze figures 7 and 8, for the detection of the 1st and 2nd MTs, respectively. In these figures we only present iterations 1 and 4 and the noise from the RoF link is tested for different values of K_{RoF}, where for each one we consider the optimal value for A_M. As expected, with the

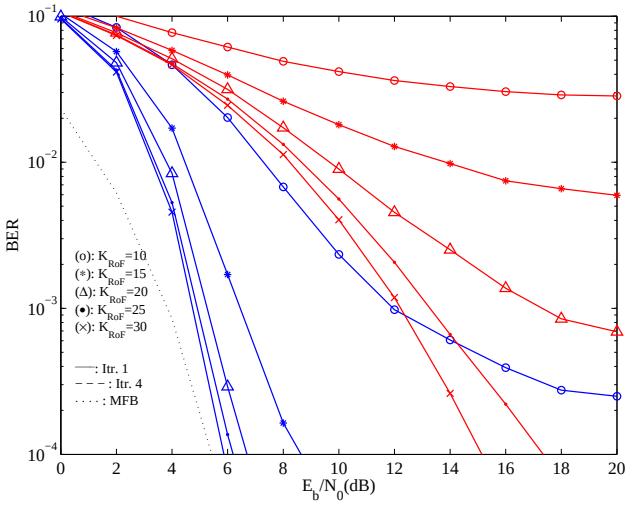

Fig. 7. BER performance for a BS cooperation scenario with $P = 2$ MTs, $R = 2$ BS and different values of K_{RoF} ($p = 1$).

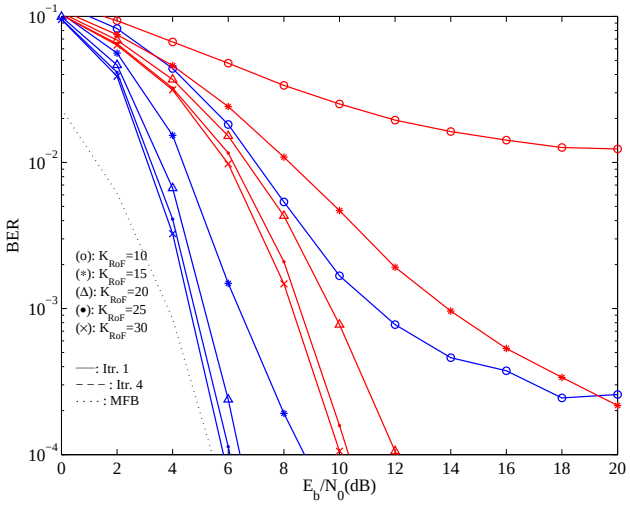

Fig. 8. BER performance for a BS cooperation scenario with $P = 2$ MTs, $R = 2$ BS and different values of K_{RoF} ($p = 2$).

increase of K_{RoF} the magnitude of noise from the RoF link decreases and the BER performance improves, stabilizing with $K_{RoF} = 20$ dB.

VI. Conclusions

This paper considered the uplink of BS cooperation systems, where the link between each BS and the CPU is performed through a RoF connection. The optical and electrical conversions are implemented by a MZ modulator and the inherent introduction of nonlinear distortion terms were presented. Moreover, an optimization on the detection scheme in order to maximize the respective SNR is presented. The proposed receiver design that takes into account both wireless and optical effects has been shown to be robust.

References

[1] C.-X. Wang, F. Haider, X. Gao, X.-H. You, Y. Yang, D. Yuan, H. Aggoune, H. Haas, S. Fletcher, and E. Hepsaydir, "Cellular Architecture and Key Technologies for 5G Wireless Communication Networks," *Communications Magazine, IEEE*, vol. 52, no. 2, pp. 122–130, Feb. 2014.

[2] D. Gesbert, S. Hanly, H. Huang, S. Shamai Shitz, O. Simeone, and W. Yu, "Multi-Cell MIMO Cooperative Networks: A New Look at Interference," *IEEE Journal on, Selected Areas in Communications*, vol. 28, no. 9, pp. 1380 –1408, Dec. 2010.

[3] L. Cimini, "Analysis and Simulation of a Digital Mobile Channel Using Orthogonal Frequency Division Multiplexing," *Communications, IEEE Transactions on*, vol. 33, no. 7, pp. 665–675, Jul 1985.

[4] H. Sari, G. Karam, and I. Jeanclaude, "An analysis of orthogonal frequency-division multiplexing for mobile radio applications," in *Vehicular Technology Conference, 1994 IEEE 44th*, Jun 1994, pp. 1635–1639 vol.3.

[5] A. Gusmão, R. Dinis, J. Conceicão, and N. Esteves, "Comparison of Two Modulation Choices for Broadband Wireless Communications," in *Vehicular Technology Conference Proceedings, 2000. VTC 2000-Spring Tokyo. 2000 IEEE 51st*, vol. 2, May 2000, pp. 1300 –1305 vol.2.

[6] D. Falconer, S. Ariyavisitakul, A. Benyamin-Seeyar, and B. Eidson, "Frequency Domain Equalization for Single-Carrier Broadband Wireless Systems," *IEEE, Communications Magazine*, vol. 40, no. 4, pp. 58–66, Apr. 2002.

[7] D. Novak, R. B. Waterhouse, A. Nirmalathas, C. Lim, P. A. Gamage, T. R. Clark, M. L. Dennis, and J. A. Nanzer, "Radio-Over-Fiber Technologies for Emerging Wireless Systems," *IEEE Journal of Quantum Electronics*, vol. 52, no. 1, pp. 1–11, Jan 2016.

[8] N. Benvenuto, R. Dinis, D. Falconer, and S. Tomasin, "Single Carrier Modulation With Nonlinear Frequency Domain Equalization: An Idea Whose Time Has Come Again," *Proceedings of the IEEE*, vol. 98, no. 1, pp. 69 –96, Jan. 2010.

[9] F. C. Ribeiro, R. Dinis, F. Cercas, and A. Silva, "Receiver Design for the Uplink of Base Station Cooperation Systems employing SC-FDE Modulations," *EURASIP Journal on Wireless Communications and Networking*, vol. 2015, no. 1, Jan. 2015.

[10] H. Kiuchi, T. Kawanishi, M. Yamada, T. Sakamoto, M. Tsuchiya, J. Amagai, and M. Izutsu, "High Extinction Ratio MachZehnder Modulator Applied to a Highly Stable Optical Signal Generator," *IEEE Transactions on Microwave Theory and Techniques*, vol. 55, no. 9, pp. 1964–1972, Sept 2007.

[11] A. Kaye, D. George, and M. Eric, "Analysis and compensation of bandpass nonlinearities for communications," *IEEE Trans. Commun.*, vol. 20, no. 5, pp. 965–972, 10 1972.

[12] H. E. Rowe, "Memoryless nonlinearities with gaussian inputs: elementary results," *The Bell System Technical Journal*, vol. 61, no. 7, pp. 1519–1525, 1982.

[13] G. Stette, "Calculation of intermodulation from a single carrier amplitude characteristic," vol. 22, no. 3, pp. 319–323, Mar. 1974.